

PCCP

Accepted Manuscript



This is an *Accepted Manuscript*, which has been through the Royal Society of Chemistry peer review process and has been accepted for publication.

Accepted Manuscripts are published online shortly after acceptance, before technical editing, formatting and proof reading. Using this free service, authors can make their results available to the community, in citable form, before we publish the edited article. We will replace this *Accepted Manuscript* with the edited and formatted *Advance Article* as soon as it is available.

You can find more information about *Accepted Manuscripts* in the [Information for Authors](#).

Please note that technical editing may introduce minor changes to the text and/or graphics, which may alter content. The journal's standard [Terms & Conditions](#) and the [Ethical guidelines](#) still apply. In no event shall the Royal Society of Chemistry be held responsible for any errors or omissions in this *Accepted Manuscript* or any consequences arising from the use of any information it contains.

Mn-modified Bi₂Ti₂O₇ Photocatalysts: A Bandgap Engineered Multifunctional Photocatalysts for Hydrogen Generation

Satyajit Gupta, Luis De Leon, Vaidyanathan (Ravi) Subramanian*

* Department of Chemical and Materials Engineering, University of Nevada, Reno, NV 89557, USA. E-mail: ravisv@unr.edu; Fax: +1 775-327-5059; Tel: +1 775-784-4686.

Abstract

In this study, a hydrogen generation photocatalyst based on bismuth titanate (Bi₂Ti₂O₇-BTO) with manganese (Mn) has been developed. Mn of varying weight percent was added to construct a modified BTO catalyst (Mn_BTO), in order to enhance the opto-electronic and photocatalytic hydrogen generation capabilities of the pristine BTO. The structural, morphological, and optical properties of the photocatalysts were evaluated by X-Ray diffractometer (XRD), scanning electron microscopy (SEM), transmission electron microscopy (TEM), and UV-visible spectrophotometer. The XRD, SEM, and TEM analysis indicates the formation of the pyrochlore BTO phase with particles of dimensions 30±10 nm. The UV-visible study revealed a reduction in the bandgap of Mn_BTO and enhanced absorption in the visible range, compared to the pristine BTO. The catalyst was optimized for maximum hydrogen generation from a water-methanol (sacrificial electron donor) system in a slurry reactor. The photocatalytic hydrogen evolution studies indicate that the Mn_BTO with up to 1 wt% Mn facilitates an optimal 140% increase in the hydrogen yield. The role of formic acid and formaldehyde as an additive in photocatalytic hydrogen evolution has also been examined. The effect of Mn content, mechanistic overview, and reusability of the catalyst is discussed.

Introduction

Hydrogen is a source of energy and is considered a clean and reliable fuel for the next generation. One of the ways of acquiring hydrogen is by light activated splitting of water, or water with sacrificial additives and a photocatalyst under solar irradiation.¹⁻⁴ This method transforms light energy to chemical energy. Various semiconductors such as titania (TiO_2),⁵ C_3N_4 ,⁶ tungsten oxide (WO_3),⁷ zirconia (ZrO_2),⁸ tantalum oxide (Ta_2O_5),⁹ strontium titanate (SrTiO_3),¹⁰ bismuth vanadate (BiVO_4),¹¹ (Oxy)nitrides¹² have been evaluated to facilitate hydrogen generation. Among these, TiO_2 is a well-studied photocatalyst.¹³⁻¹⁸ Various modifications/doping have been investigated including carbon/nitrogen¹⁹ doped TiO_2 , noble metal-oxide composites ($\text{Pt-TiO}_2/\text{Au-TiO}_2/\text{Ag-TiO}_2$)²⁰⁻²³ and several transition metal ion doped titania²⁴ in an effort to improve photocatalytic activity. Noble metal-based SrTiO_3 has also been studied²⁵ for improvement in the photocatalytic activity. The effect of different salts on various photocatalysts during hydrogen evaluation has also been carried out.²⁶ Recently, inverse opal structured hematite ($\alpha\text{-Fe}_2\text{O}_3$)²⁷ has been developed as a photoanode for photoelectrochemical water splitting. Electrophoretic deposition of colloidal hematite as a photoanode was also carried out for water splitting.²⁸

BTO ($\text{Bi}_2\text{Ti}_2\text{O}_7$) is a low bandgap semiconductor and a visible light-driven photocatalyst for hydrogen generation,²⁹ but its ability to function as a composite with other additives and the resulting properties are not well understood. Fundamentally, BTO ($\text{Bi}_2\text{Ti}_2\text{O}_7\text{-A}_2\text{B}_2\text{O}_7$) has a pyrochlore type structure (consisting of an interpenetrating cuprite (A_2O) tetrahedral with corner sharing BO_6 octahedron),³⁰ where the A and B sites can be altered by various elements³¹ causing a small structural distortion. As a comparison, the bandgap of TiO_2 [bandgap of 3.2 eV (for anatase) and 3.0 eV (for rutile)] is larger than BTO (band gap of 2.8 eV). The large band gap of TiO_2 restricts the photocatalytic application to the UV domain only (sunlight contains only 4% UV light). Hence it is important to develop a broad spectrum absorption catalyst that can absorb in the visible and also demonstrates chemical stability similar to the TiO_2 . Compared to TiO_2 , BTO based materials show increased absorbance in the visible spectrum.²⁹

Previously, theoretical modeling of BTO was investigated, based on pseudo-potential plane wave calculations and substitution of BTO by various d-block elements (Fe, Mn, Cr, Ni), in order to understand their electronic effects.³² It was shown that a reduction in the bandgap of BTO is due to the $6s^2$ electrons of bismuth (these electrons also responsible for the inert pair

effect observed in Bi) helping to reduce the band gap as observed from the electronic structure. Not only is it the contribution of $6s^2$ electrons, PDOS (partial density of states) investigation of individual atoms of BTO further confirms that bismuth helps in the enhancement of the 'p' type character of the conduction band (valence band of BTO has a good 'p' character due to the contribution of oxygen 2p). These two synergistic effects of Bi assist in up-shifting the valence band towards conduction band and help to promote the electron transfer during photo excitation. It was also observed that the percentage of the p-character is 7% more in BTO (21.68%) than TiO_2 (14.32%). These observations imply that BTO is a promising broad spectrum absorption photocatalyst that is amenable for further modification and applied to photocatalytic reactions.

The theoretical investigation also indicated that there are multiple ways by which the bandgap of BTO can be further reduced and its light absorption properties can be improved. Specifically, doping of manganese in the BTO structure is one of the possible approaches to improve the light absorption in the visible domain. The substitution of this dopant can create interband states, which can help in the charge transfer from the valence band to the conduction band. It is notable to mention that CdS with a band gap of 2.4 eV (similar to BTO onset absorption) can absorb in the visible domain but the material is unstable and toxic. Alternately, coupling of various co-catalysts and a visible light absorber (sensitization) to form a composite have been used to improve the activity of TiO_2 in the visible region.

Unlike such multicomponent additive structure, this work illustrates the designing of a single structure. In order to enhance the visible light absorption and boost the photocatalytic activity, a modification of BTO using manganese (Mn_BTO) was examined. A wet chemical approach was followed to synthesize the photocatalyst. Non-toxic, environmentally benign, and earth abundant precursors were used to build up a '*bandgap engineered composite oxide nanocatalyst (BECON)*' system that can demonstrate a proof of concept generation of hydrogen from various pollutants under light irradiation. The catalysts showed an improvement in the visible light absorption with an increase in the manganese content. The photocatalytic hydrogen generation carried out with the synthesized catalysts in a slurry reactor demonstrates an improvement in the hydrogen production until a critical concentration of manganese was reached.

1. Experimental

1.1. Materials

Bismuth (III) nitrate pentahydrate and manganese (II) acetate tetrahydrate were obtained from Alfa Aesar and used as a precursor. Titanium (IV) iso-propoxide (97%), acetonitrile and Triton X were obtained from Sigma Aldrich (St. Luis MO). Nitric acid (ACS, BDH3046-2.5LPC, 68%) and ammonia solution (A667-212, 27-31% ammonia solution in water and density of 0.91 g ml⁻¹) were obtained from BDH Aristar and Fisher Scientific respectively. UHP deionized water was obtained using a Millipore water purification system and used for the synthesis. The chemicals were used without further purification.

1.2. Synthesis

Titanium isopropoxide was converted to 0.1 M titanium nitrate by hydrolysis using nitric acid. In a typical procedure, first the precursor was hydrolyzed in water, to form white precipitate of titanium oxohydroxide/hydroxide species [TiO(OH)₂/Ti(OH)₄]. The precipitate was dissolved in concentrated nitric acid with ultra-sonication, followed by the addition of water to maintain an acid concentration of 1 M. This solution was used immediately as a titanium precursor for the BTO synthesis. Bismuth nitrate and manganese nitrate stock solutions of 0.1 M concentration were prepared by dissolving respective salts in nitric acid of 1 M concentration.

BTO was synthesized by a co-precipitation method, followed by annealing (Scheme 1). Different groups have synthesized BTO by various techniques such as, solvothermal,³³ sol-gel,³⁴ chemical solution decomposition method,³⁵ co-precipitation followed by microwave sintering³⁶ techniques. In this study, the synthetic procedure followed is based on co-precipitation of the respective salts followed by calcination in a furnace at 600°C, which is described in scheme 1. Co-precipitation method is a simple and cost-effective technique that provides a better control on the particle size and it does not require any third component/template as is the case with some other methods.

Equal volumes (50 ml) of the titanium precursor and bismuth nitrate were added to a 250 mL beaker. Manganese acetate solution [(0.5×X) ml, where, X is the % of Mn²⁺; X=0 for pristine BTO] was added in an equal volume, in place of Bi solution [50-(0.5×X)] and was mixed uniformly. After mixing, ~50 mL of strong ammonium hydroxide solution was added with stirring to this beaker to precipitate out all of the dissolved metals in the form of hydroxides [pH=12]. Once the precipitate settled, the supernatant was removed. The precipitate was then

collected by centrifugation and washed thoroughly with deionized water. The solid gel-like precipitate was then oven dried at 150°C for 2 h. The dried mass was crushed into fine powder using a mortar and pestle and was transferred to a small crucible. This crucible was placed inside a larger crucible containing bismuth oxide at the bottom. The larger crucible was capped to ensure the availability of high Bi vapor pressure (Scheme 1).

The furnace temperature was increased from 25°C to 600°C in 2 h, maintained constant at that temperature for 4 h, and then decreased to 25°C in 1 h. The Lindberg[®] Bluebox furnace (from Thermo Fisher Scientific) with programmable temperature controller was used for this process. As a control, pristine BTO was synthesized by following the same procedure mentioned above but without introducing any manganese additives. The catalysts are labeled as following this point forward: BTO, Mn_BTO0.5, Mn_BTO1, Mn_BTO2 and Mn_BTO3. These names respectively correspond to pristine BTO, 0.5%, 1%, 2% and 3% Mn salt by weight at the time of the synthesis.

1.3. Characterization

1.3a Surface, morphological, and optical characterization

Phase analysis of the synthesized photo-catalysts was carried out using an XRD instrument [Philips (model: 12045 B/3X-ray diffractometer) with a scan rate of 0.03°/min and Cu K-alpha was used as X-ray source]. A Hitachi[®]S-4700 scanning electron microscope (SEM) was used to determine the surface features of the as synthesized BTO powder. For the SEM studies the particles were dispersed in ethanol and drop casted over carbon tape and observed under an accelerating voltage of 3 kV. A JEOL[®] 2100F high resolution transmission electron microscope (HRTEM) was used to examine the morphological features of the samples (*Resolution*: Point 0.23 nm, Lattice 0.1 nm, *Electron gun*: Field emission ZrO/W (100), *Acc. Voltage*: 200 kV). ICP-OES (Perkin Elmer[®] Optima 5300) of the catalysts were carried out using Perkinelmer[®] to understand the variation of the concentration of Mn in the catalysts. The optical absorption properties of the BTO and Mn_BTO were examined using a UV-visible spectrophotometer (Shimadzu UV-2501PC) with a wavelength variation from 300 to 800 nm. In order to study the absorption properties, the powders were first dispersed in a solution containing an acetonitrile/water mixture. Then the surfactant, Triton X was added and it was coated over the glass slides and heated to 400 °C to burn the organics off and obtain uniform films. The films were used in the absorbance measurements.

1.3b Photo-catalytic slurry reactor for the H₂ evaluation

The H₂ generation experiments were carried out in a slurry reactor connected with a high pressure mercury lamp. A 500 ml capacity slurry reactor (contains a reactor, concentric quartz tube with water circulation, and a power source) was purchased from Ace Glass[®], Vineland, NJ. A immersion-type medium pressure quartz mercury lamp was also purchased from Ace Glass. The lamp has a maximum energy output in the visible range (further details are given in the supporting information, Fig. S1, Section-A). The reactor configuration and setup is shown in Fig. S1 (See ESI†). 0.15 g of the catalyst was mixed with 250 ml water and 50 ml of methanol (the amount of the catalyst was optimized initially). Argon gas was sufficiently purged for at least 20 min to remove any dissolved gas species. Under the radiation, the gas produced due to the photocatalytic process was collected by a process involving downward displacement of a water column. The quantitative analysis of the gas (at a pressure of 1.003 atm and temperature of 27°C) collected at various intervals of time was carried out using gas chromatograph. The amount of the hydrogen evolved was determined using a SRI GC model 8610C, Multi gas channel #3 with a TCD detector. The cumulative hydrogen yield is calculated by the summation of the amount of hydrogen evolved at various interval of time over 130 min. (~ 2.16 hr). This helps to understand the total hydrogen generated by the respective catalysts, within the time window of 130 min.

2. Results and discussions

2.1 Structural analysis of the catalysts: XRD

The phase analysis of the synthesized powders was performed by examining the XRD results, shown in Fig. 1. XRD illustrates the presence of several peaks of the synthesized material. The presence of multiple peaks in the XRD with large signal-to-noise ratio indicates that the material is crystalline. The diffraction pattern in the XRD corresponds to the pyrochlore phase bismuth titanate (Bi₂Ti₂O₇-BTO) as indicated by the reference JCPDS Card # 32-0118. The XRD shows a peak at 28.7°, which corresponds to the (622) *hkl* plane, 29.9° which corresponds to the (444) *hkl* plane, and 35° which corresponds to the (800) *hkl* plane (other peaks are indexed likewise). The key 100% peak at 29.9° corresponding to the 444 (*hkl*) plane indicates that the as synthesized Mn_BTO reveals a pyrochlore phase. The representative XRD patterns of BTO synthesized in the presence of varying Mn content are also shown. Furthermore the equation, crystallite size = $0.89\lambda/\beta\cos\theta$ where β = full-width half-maximum (FWHM) of the

main diffraction peak and $\lambda =$ the Cu radiation, was used. For BTO, the crystallite size was observed to be 24 nm, while for the Mn_BTO1 it was 22.1 nm.

2.2. Morphological analysis of the catalysts: SEM and TEM

The morphology and size of the particles were examined using scanning electron microscopy (Fig. 2). This analysis shows that the BTO particles exhibit a uniform architecture with particle size diameter of 30 ± 10 nm. The SEM images of two Mn_BTO samples are shown in Fig. 2. The synthesized Mn_BTO also shows particle size similar to the BTO. The observation indicates that the addition of manganese slightly alters the particle features making them finer and more spherical in shape, but leaves them generally spherical. The general resemblance in the physical features of the particles is a desirable feature since it ensures that a comparison of the photocatalytic activity will not be clouded significantly by variation in the particle features. In previous studies it was observed that thermal treatment method can be used as a robust and standalone strategy for the control of particle shape and agglomerate size.³⁷

The Mn_BTO particles were further characterized using HRTEM (high resolution transmission electron microscopy). A multiparticle HRTEM image and a close-up of a single particle image of Mn_BTO1 is shown in Fig. 3A. The image shows a particle size distribution of $\sim 25 \pm 5$ nm, which is in a close agreement with the SEM analysis. The high resolution fast Fourier transformation (FFT) analysis (Fig. 3B) indicates a “*d-spacing*” value of 2.95 Å, corresponding to the 444 plane of the BTO. The clear lattice fringes can be observed from the HRTEM image (Fig. 3B), which suggests a ordering with a high degree of crystallinity. The high resolution fast Fourier transformation (FFT) analysis indicates the crystalline nature of the synthesized nanoparticles (Fig. 3B Inset). Further, to understand the distribution of ‘Mn’ in the samples, ICP-OES analysis was carried out with the catalysts. This analysis provided a concentration (in PPM units) value of 0.08 ± 0.01 for Mn_BTO1 and a concentration (PPM) of 0.16 for Mn_BTO2 indicating that the concentration gradually increases with the increase in the Mn content during the synthesis of the catalysts.

2.3. Optical properties of the photocatalysts: UV-visible analysis

The absorbance spectra of the BTO and Mn_BTO samples were examined to get an insight into the optical characteristics of these materials. The bandgap was calculated from the UV-visible absorbance spectra (Fig. 4A),³⁷ using the expression, $E_g = hc/\lambda$, where, E_g is the optical band gap, h is the Planck’s constant, λ is wavelength corresponding to the onset of absorbance,

and c is the velocity of light. In the case of BTO, the bandgap was estimated as 2.8 eV (Fig. 4A,a). Compared to BTO, Mn_BTO0.5 showed a red-shift in the absorbance by 50 nm. Increasing the concentration of Mn, shifted the onset of absorbance by a maximum of 230 nm, in the case of Mn_BTO3 (Fig.4A, b-e). It can be observed that there is a linear decrease in the band gap with an increase in the concentration of manganese (Fig 4B).

An earlier modeling analysis of Mn_BTO has indicated that the reduction in bandgap is due to the formation of an intermediate state above the valence band.³² The 'd⁵' electrons of Mn²⁺, is responsible for the formation of this interband state since the valence band of BTO is formed mainly by the 'd' orbitals of Ti. It is understood that this arrangement facilitates efficient electrons transit from the impurity level formed by Mn above VB to the CB. The ensuing redshift in the absorbance is also in accordance to our previous theoretical predictions.³² A collage of photographs with various Mn content is shown in the Fig. 4A (Inset). It indicates a gradual change in color and is consistent with absorbance studies.

2.4. Effect of percent Mn loading on the hydrogen generation

The photocatalytic hydrogen generation studies were carried out using a slurry reactor. All the synthesized photocatalysts demonstrated hydrogen generation from a water/methanol mixture (Fig. 5). As compared to the BTO, the manganese incorporated samples showed an improvement in hydrogen yield. A 50% increase in the hydrogen yield was observed with minimal Mn content (Mn_BTO0.5) and a maximum of ~140% increase in the hydrogen yield relative to BTO was observed with Mn_BTO1 (Fig. 6). Any further increase in the Mn content was found detrimental and resulted in a decrease in the hydrogen yield; though this yield was still higher than BTO. The decrease in hydrogen yield with the increase in the Mn concentration can be attributed to the increase in the charge recombination sites as indicated below.

Higher concentration of d-block elements such as iron can be detrimental in that they often act as a charge recombination center. For example, in a related study, excessive amount of Fe in TiO₂ has shown a similar behavior towards photooxidation of 2 propanol to acetone, in which the key step is the photoexcitation.³⁸ In our system, excess of Mn in the Mn_BTO function as recombination centers effectively reducing the number of holes and electrons generated during the photocatalytic reaction. As a result, there is a net reduction in the photogenerated charges available at the catalyst surface for redox reactions.

2.5. Effect of methanol concentration

The effect of methanol concentration was systematically examined by varying the water/methanol ratio (water/methanol (v/v)- 300/0, 250/50, 200/100, 150/150, 50/250, 0/300) using the catalyst 'Mn_BTO1'. An increasing methanol concentration showed an increase in the hydrogen yield (Fig. S2, See ESI†). This observation is attributed to improved reactivity of CH₃OH relative to water. CH₃OH becomes more reactive because of the accumulation of negative charge on the oxygen (due to the inductive effect of -CH₃). Because of this effect, methanol readily reacts with the generated holes and is preferentially consumed to form hydrogen ions (for this reason, CH₃OH is also referred to as a sacrificial agent) and thereby generates more hydrogen by the reduction of electrons from the conduction band.

2.6. Amount of catalyst optimization

The catalyst amount was optimized for the Mn_BTO sample showing the best hydrogen yield based on the studies in section 2.5. The results shown in Fig. 7 indicate that with the increasing catalyst amount there is an increase in hydrogen yield till a maximum of 0.15 g catalyst loading is reached. Any further increase in the catalyst loading results in a decrease in hydrogen production. This decrease is attributed to the undesirable light scattering effect or shadowing of light caused by the turbidity of the solution common in photocatalysts using a slurry reactor configuration.³⁹ These effects decrease the effective incident light for photoexcitation of the charges and significantly decrease the number of electrons-holes that are generated for sustaining the photocatalytic reaction. 0.15 g of catalyst was found to be optimum for photocatalytic hydrogen generation and was therefore used in subsequent experiments.

2.7. Effect of additives, formaldehyde and formic acid (H₂ generation from pollutants)

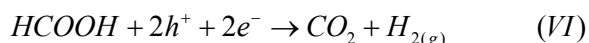
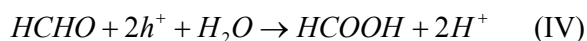
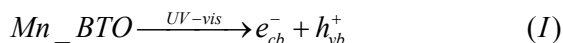
The Mn_BTO photocatalysts were further tested for their role towards hydrogen generation from various additives such as formaldehyde and formic acid. These additives are considered for two reasons: They are reported as byproducts/intermediates of methanol conversion⁴⁰ and are also considered as industrial waste products or model pollutants.⁴¹ The experiments were carried out using a mixture of water/additive (250/50 v/v) and a catalyst loading of 0.15 g. Hydrogen evolution was noted with all the additives as indicated in Fig. 8. The cumulative hydrogen yield in 2.16 h was two orders of magnitude higher for formic acid (32.5 ml g⁻¹) than formaldehyde (0.6 ml g⁻¹). While this shows that the photocatalysts can be used to decompose various pollutants, it also alludes to the existence of a preferential pathway to produce hydrogen via formic acid.

2.8. Mechanistic details

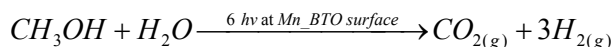
The photocatalytic oxidation reaction in the presence of methanol is detailed here. Methanol first undergoes hole mediated oxidation to formaldehyde (dissociation energy of 47.8 KJ mol⁻¹) and releases two protons [H⁺] (Eqn. I). These protons react with the electrons (e⁻) from the conduction band to generate hydrogen (Eqn. II). Meanwhile, the formaldehyde further oxidizes to formic acid (dissociation energy of -95.8 KJ mol⁻¹) as shown in Eqn. III, releasing a single [H⁺]. It is interesting to note that the nature of the hydrogen evolution shows an initial slow rate (till 70 min) and then a rapid increase with a greater slope reflecting increased rate (>70 min) in the hydrogen evolution. In the methanol system, the formation of formaldehyde and formic acid indicates that all of these reactions are competitive. However, the formic acid is responsible for the increased rate of hydrogen, as explained below.

The experiments of section 2.7 with water/formaldehyde (A) and water/formic acid (B) were carried out to further understand this process. In the case of (A) an inflection point was observed with a low hydrogen yield (0.6 ml g⁻¹). In the case of (B), the large hydrogen yield was observed (32.5 ml g⁻¹). In the first case (A), at the beginning stage, formaldehyde oxidizes to formic acid (Eqn. IV), generating a low amount of hydrogen. After that, at the inflection point, formic acid generation occurs which then accumulates, and is finally oxidized to produce hydrogen (Eqn. V). In the case of B, a huge amount of hydrogen is produced in the early stage. This explains that in case of methanol, initially it converts to formaldehyde, which generates a small amount of hydrogen. The formaldehyde then converts to formic acid which results in a large hydrogen yield as, -COOH group of formic acid dissociates thermodynamically and spontaneously due to low dissociation energy (-95.8 KJ mol⁻¹) compared to methanol (64.1 KJ mol⁻¹) and formaldehyde (47.8 KJ mol⁻¹).⁴²

The aforementioned photocatalytic oxidation reactions can be summarized as follows,



Overall,



The beginning stage consists of methanol oxidizing to formaldehyde (A). After a substantial accumulation of formaldehyde, the formaldehyde is oxidized to formic acid. Consequently formic acid oxidizes to yield a large amount of hydrogen as observed in the later segment of the time resolved hydrogen yield analysis. At this stage the dissolved hydrogen also exceeds the saturation limit and that comes out of the solution.

The results indicate that BTO is amenable to bandgap modulation with promising activity towards photocatalysis. The catalysts have shown that it can be used for simultaneous multifunctional applications such as clean fuel (hydrogen) generation as well as pollutant (formic acid, formaldehyde) photodegradation.

2.9. Reusability of the catalyst

In order to verify the stability of the photocatalysts, reusability studies were performed. Both photocatalytic and surface analysis of the same batch of photocatalysts were systematically carried out. The used photocatalyst were collected by centrifugation after the 1st run, dried in air, and subsequently reused with a fresh batch of methanol-water mixture. It is to be noted that some of the photocatalyst was lost during the centrifugation and not recoverable. The repeat use in a 2nd run shows that there is a reduction in the hydrogen yield by approximately 33% (Fig. 9). The process was repeated again (recovering catalyst and reusing in a 3rd run). At this time the loss of activity was much smaller (~3%) as indicated in the Fig. 9.

In order to investigate this reduction in activity the catalysts were analyzed by SEM, XRD, and FTIR spectroscopic technique. XRD and SEM results indicated no disintegration or change in the morphology and particle size (Fig. S3 and Fig. S4, See ESI†). This observation rules out any physical attrition or change of phase. However, the FTIR spectra of the reused catalyst showed additional peaks before and after subjected to photo-catalytic reaction (Fig. S5, See ESI†). These additional peaks, correspond to methoxy (-OMe), carbonyl (-C=O) and aliphatic regions. The surface coverage by carbonyl fragment confirms that the reaction proceeds through the 'formaldehyde-formic acid intermediate' (Eq II and IV) pathway discussed in the previous section. The surface coverage of the used catalyst by methoxy (-OCH₃) and other functional groups suggest that there is a considerable reduction of the available active sites as per the mechanism shown in Fig. 8 (Inset). These groups hinder the reaction of methanol molecules at the surface and results in a decrease in hydrogen yield. A similar observation was noted in a gas phase photocatalytic conversion of hydrogen from methanol and water using TiO₂ as a catalyst.⁴³

The fact, that the 3rd run showed only a further 3% reduction in hydrogen yield as compared to 2nd run, indicates that the effective surface of the catalyst remained the same as that observed after the 2nd run. It is likely that the steric factor from preadsorbed groups does not allow other species to adsorb onto the catalyst surface.

3. Conclusions

A series of Mn_BTO photocatalysts were developed by implementing a wet chemical route. The Mn modified catalysts showed a redshift in the absorption of upto a 100 nm in Mn_BTO3 (3 wt% Mn), compared to pristine BTO. An increase in the Mn loading till a critical concentration of 1 wt% showed a ~140% increase in the photocatalytic hydrogen production, compared to pristine BTO. Higher concentrations of Mn can act a recombination center for photogenerated charges and effectively reduces the hydrogen yield compared to Mn_BTO1. However, Mn_BTO3 still yields more hydrogen (~22% higher) compared to pristine BTO. Separate studies with aqueous formic acid and formaldehyde solutions assist in sheading light into the mechanism of hydrogen evolution. Acceleration in the hydrogen yield is attributed to the formation of formic acid (intermediate of methanol photooxidation). A 33% reduction noted during reusability studies can be attributed to the surface coverage by various groups as evidenced from FTIR analysis, leading to a blockage of active centers of the photocatalyst. The catalyst showed an insignificant reduction in subsequent run. The evidence of hydrogen generation from methanol, formic acid, and formaldehyde indicates that Mn_BTO can be used as a versatile multifunctional photocatalyst for environmental remediation as well as clean fuel production.

Acknowledgements

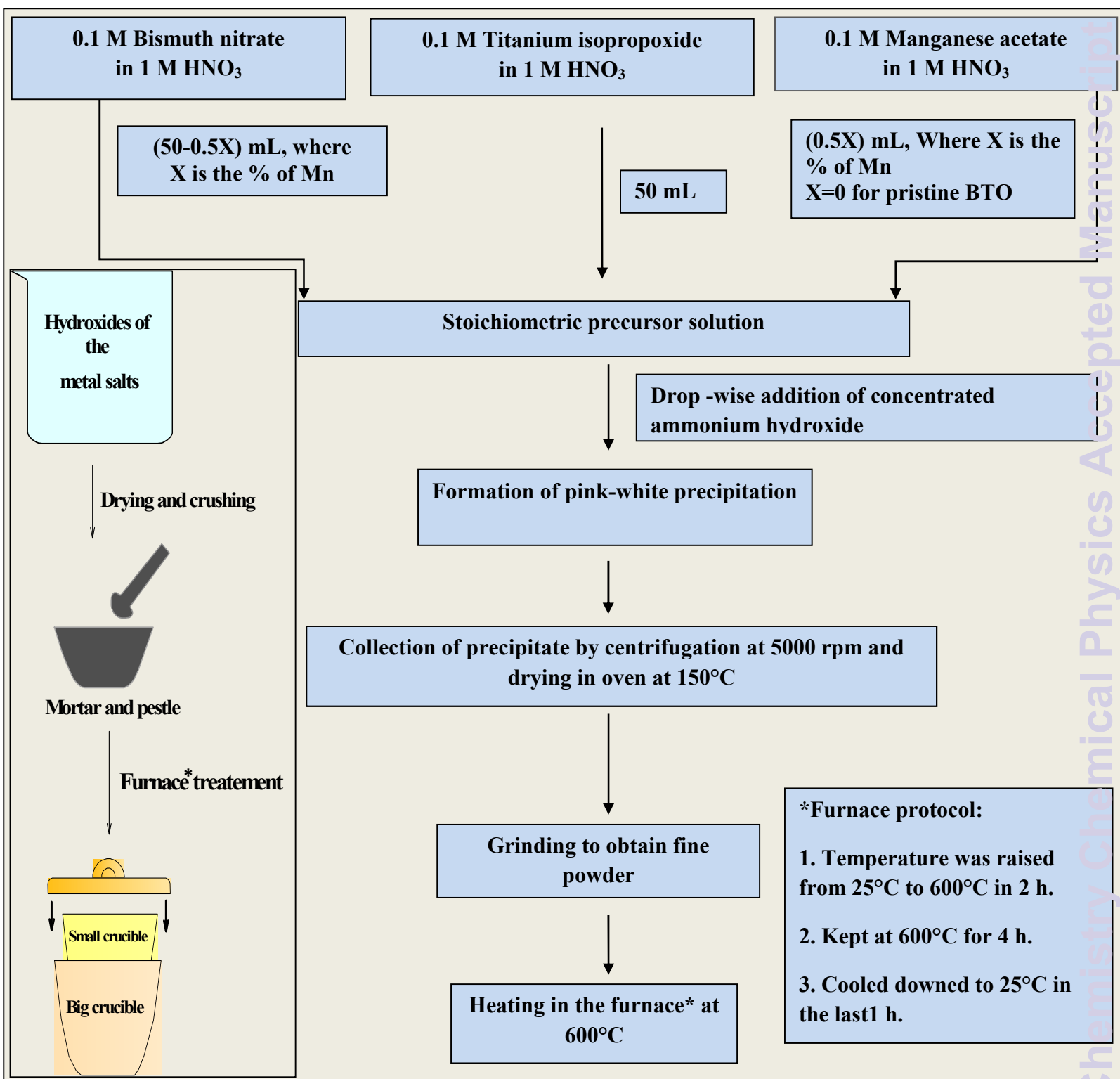
The authors gratefully thank Brad Allured and Bill Ragsdale, University of Nevada for helpful insights and discussions. RSV thanks Swagotom Sarker for SEM studies and Dr. Mo Ahmedian for HRTEM studies. NSF funding (NSF-CBET 1134486) is also acknowledged.

† **Electronic supplementary information (ESI) available.** See DOI: 10.1039

Notes and references

- 1 Y. Horiuchi, T. Toyao, M. Takeuchi, M. Matsuoka and M. Anpo, *Phys. Chem. Chem. Phys.*, 2013, **15**, 13243.
- 2 A. Kudo, *Pure Appl. Chem.*, 2007, **79**, 1917.
- 3 M. Ni, M. K.H. Leung, D. Y. C. Leung and K. Sumathy, *Renewable and Sustainable Energy Reviews*, 2007, **11**, 401.
- 4 A. Valdes, J. Brillet, M. Gratzel, H. Gudmundsdottir, H. A. Hansen, H. Jonsson, P. Klupfel, G. J. Kroes, F. L. Formal, I. C. Man, R. S. Martins, J. K. Norskov, J. Rossmeisl, K. Sivula, A. Vojvodic and M. Zach, *Phys. Chem. Chem. Phys.*, 2012, **14**, 49.
- 5 M. A. Lazar and W. A. Daoud, *RSC Adv.*, 2013, **3**, 41.
- 6 X. C. Wang, K. Maeda, A. Thomas, K. Takanabe, G. Xin, J. M. Carlsson, K. Domen and M. Antonietti, *Nat. Mater.*, 2008, **8**, 76.
- 7 X. Liu, F. Wang and Q. Wang, *Phys. Chem. Chem. Phys.*, 2012, **14**, 7894.
- 8 S. Poliseti, P. A. Deshpande, and G. Madras, *Ind. Eng. Chem. Res.* 2011, **50**, 12915.
9. R. V. Goncalves, P. Migowski, H. Wender, D. Eberhardt, D. E. Weibel, F. C. Sonaglio, M. J. M. Zapata, J. Dupont, A. F. Feil, and S. R. Teixeira, *J. Phys. Chem. C* 2012, **116**, 14022.
- 10 H. Yu, J. Wang, S. Yan, T. Yu and Z. Zou, *J. of Photochem. Photobiol. A: Chem.* 2014, **275**, 65.
- 11 A. Iwase and A. Kudo, *J. Mater. Chem.*, 2010, **20**, 7536.
- 12 K. Maeda, *Phys. Chem. Chem. Phys.*, 2013, **15**, 10537.
- 13 P.V. Kamat, *Chem. Rev.*, 1993, **93**, 267.
- 14 A. Heller, *Acc. Chem. Res.*, 1995, **28**, 503.
- 15 N. Li, X. Lang, W. Ma, H. Ji, C. Chen and J. Zhao, *Chem. Commun.*, 2013, **49**, 5034.
- 16 R. Daghrir, P. Drogui and D. Robert, *Ind. Eng. Chem. Res.*, 2013, **52**, 3581.
- 17 X. Chen and S. S. Mao, *Chem. Rev.*, 2007, **107**, 2891.
- 18 A. Fujishima, T. N. Rao and D. A. Tryk, *J. Photochem. Photobiol. C: Photochem. Rev.*, 2000, **1**, 1.
- 19 R. Asahi, T. Morikawa, T. Ohwaki, K. Aoki and Y. Taga, *Science*, 2001, **293**, 269.
- 20 B. Naik, S. M. Kim, C. H. Jung, S. Yi Moon, S. H. Kim and J. Young, *Adv. Mater. Interfaces*, 2014, **1**, 1300018.
- 21 J. Xing, J. F. Chen, Y. H. Li, W. T. Yuan, Y. Zhou, L. R. Zheng, H. F. Wang, P. Hu, Y. Wang, H. J. Zhao, Y. Wang and H. G. Yang, *Chem. Eur. J.*, 2014, **20**, 2138.

- 22 V. Subramanian, E. E. Wolf and P. V. Kamat, *J. Am. Chem. Soc.*, 2004, **126**, 4943.
- 23 A. Bumajdad and M. Madkour, *Phys. Chem. Chem. Phys.*, 2014, DOI: 10.1039/c3cp54411g.
- 24 H. Yamashita, M. Harada, J. Misaka, M. Takeuchi, K. Ikeue and M. Anpo, *J. Photochem. Photobiol. A: Chem*, 2002, **148**, 257.
- 25 V. Subramanian, R. K. Roeder and E. E. Wolf, *Ind. Eng. Chem. Res.*, 2006, **45**, 2187.
- 26 K. Sayarna and H. Arakawa, *J. Photochem. Photobiol. A: Chem.*, 1996, **94**, 67.
- 27 X. Shi, K. Zhang, K. Shin, J. H. Moon, T. W. Lee and J. H. Park, *Phys. Chem. Chem. Phys.*, 2013, **15**, 11717.
- 28 X. Zong, S. Thaweesak, H. Xu, Z. Xing, J. Zou, G. Lua and L. Wang, *Phys. Chem. Chem. Phys.*, 2013, **15**, 12314.
- 29 S. Murugesan and V. Subramanian, *Chem. Commun.*, 2009, 5109.
- 30 M. A. Subramanian, G. Aravamudan and G. V. S. Rao, *Prog. Solid State Chem.*, 15, **1983**, 55.
- 31 A. Kudo, H. Kato and S. Nakagawa, *J. Phys. Chem. B*, 104, **2000**, 571.
- 32 S. Murugesan, M. N. Huda, Y. Yan, M. M. Al-Jassim and V. Subramanian, *J. Phys. Chem. C*, 2010, **114**, 10598.
- 33 J. Ren, G. Liu, Y. Wang and Q. Shi, *Mat. Let.*, 2012, **76**, 184.
- 34 J. Q. Hu, Y. Yu, H. Guo, Z. W. Chen, A. Q. Li and X. M. Feng, *J. Mater. Chem.*, 2011, **21**, 5352.
- 35 W. F. Yao, H. Wang, X. H. Xua, J. T. Zhou, X. N. Yang, Y. Zhang and S. X. Shang, *Applied Catalysis A: General*, 2004, **259**, 29.
- 36 J. R. E. Elizondo, B. B. Hinojosa and J. C. Nino, *Chem. Mater.*, 2011, **23**, 4965.
- 37 B. Allured, S. Delacruz, T. Darling, M. N. Huda and V. Subramanian, *Appl. Catal. B: Environmental*, 2014, **144**, 261.
- 38 H. Yamashita, M. Harada, J. Misaka, M. Takeuchi, B. Neppolian and M. Anpo, *Catal. Today*, 2003, **84**, 191.
- 39 R. Bhosale, S. Pujari, G. Muley, B. Pagare and A. Gambhire, *J. Nanostructure in Chem.*, 2013, **3**, 46.
- 40 J. Chen, D. F. Ollis, W. H. Rulkens and H. Bruning, *Wat. Res.*, 1999, **33**, 669.
- 41 X. Chen, S. Shen, L. Guo and S. S. Mao, *Chem. Rev.*, 2010, **110**, 6503.
- 42 H. J. Choi and M. Kang, *Int. J. Hydrogen Energy*, 2007, **32**, 3841.
- 43 M. Kawai, S. Naito and K. Tamaru, *Chem. Phys. Lett.*, 1983, **98**, 377.



Scheme 1 The schematic indicates the *step-by-step* details applied for the synthesis of bismuth titanate (BTO) and Mn_xBTO, with varying Mn content.

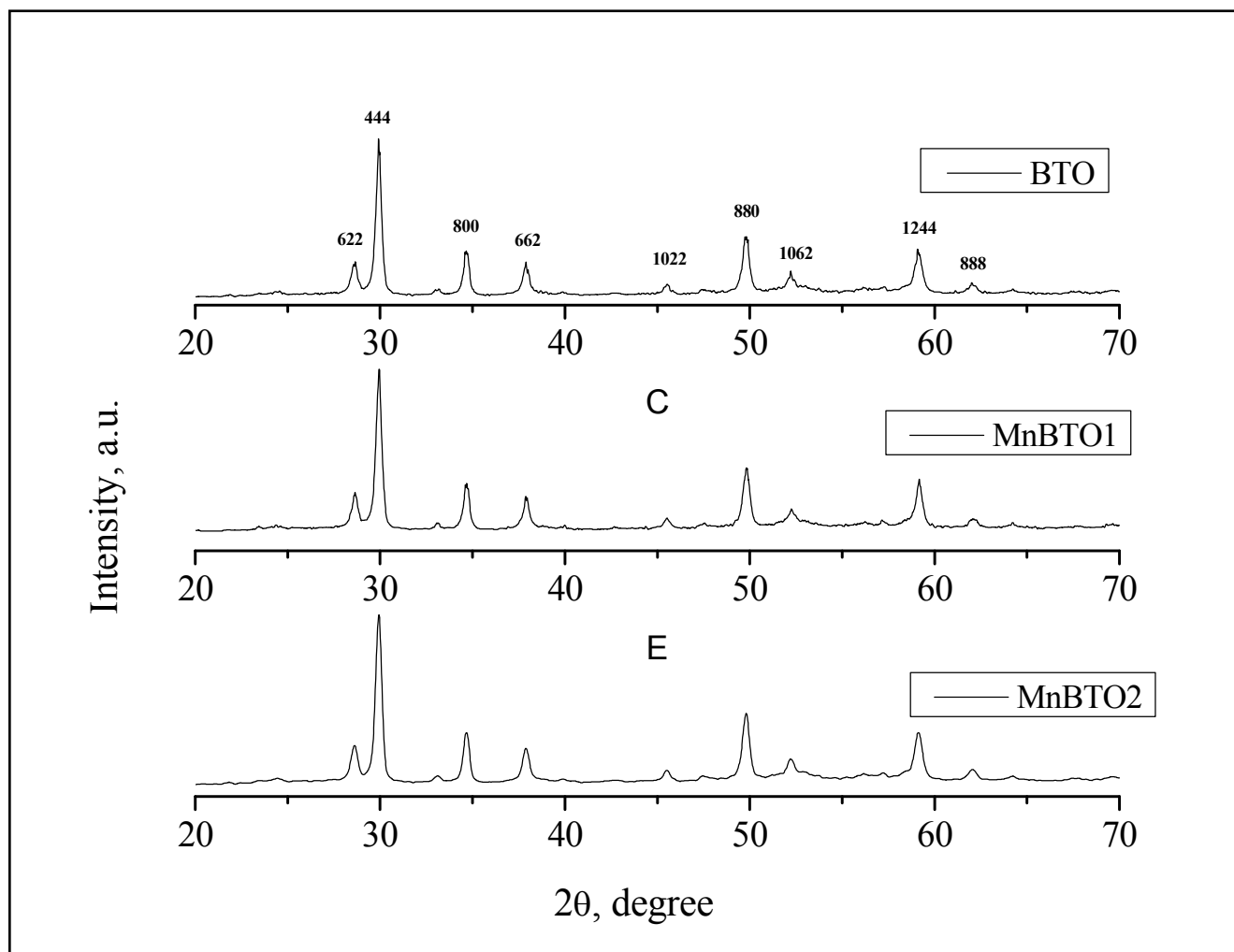


Fig. 1 The XRD of the as synthesized BTO, BTO with 1 wt % Mn (Mn_BTO1), and 2 wt % Mn (Mn_BTO2) are shown. The diffractograms were obtained using a scan rate of 0.03°/min.

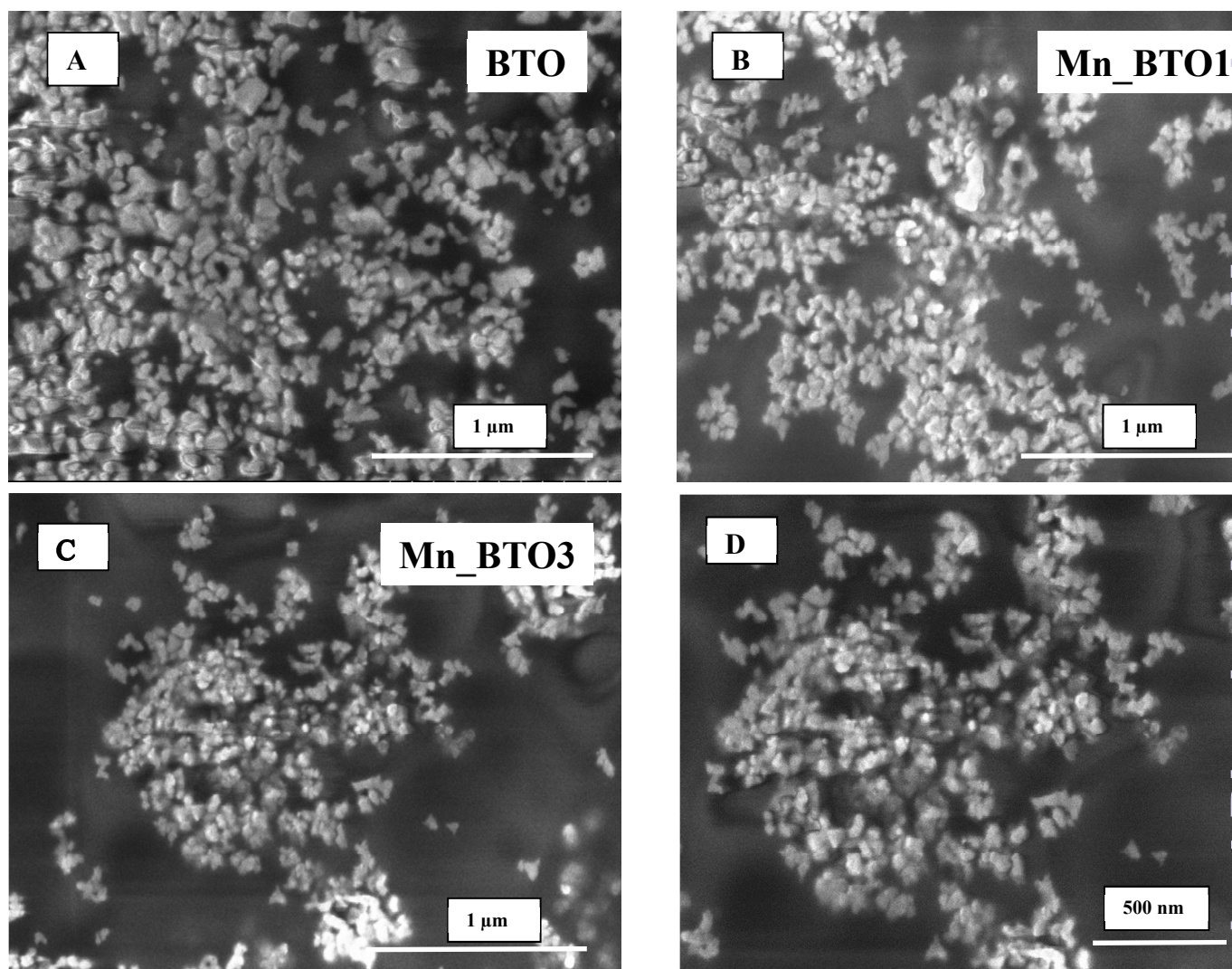


Fig. 2 The SEM images of (A) BTO, BTO with a varying Mn content (B) 1 wt% (Mn_BTO1), (C) 3 wt % (Mn_BTO3), and (D) Mn_BTO3 with higher magnification.

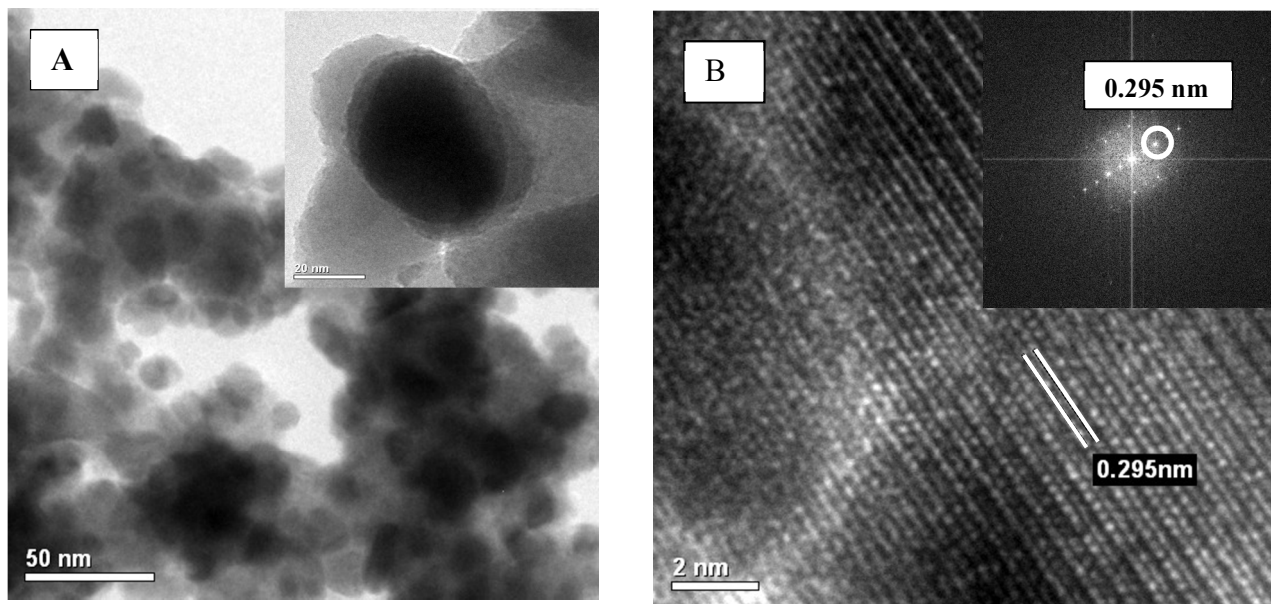
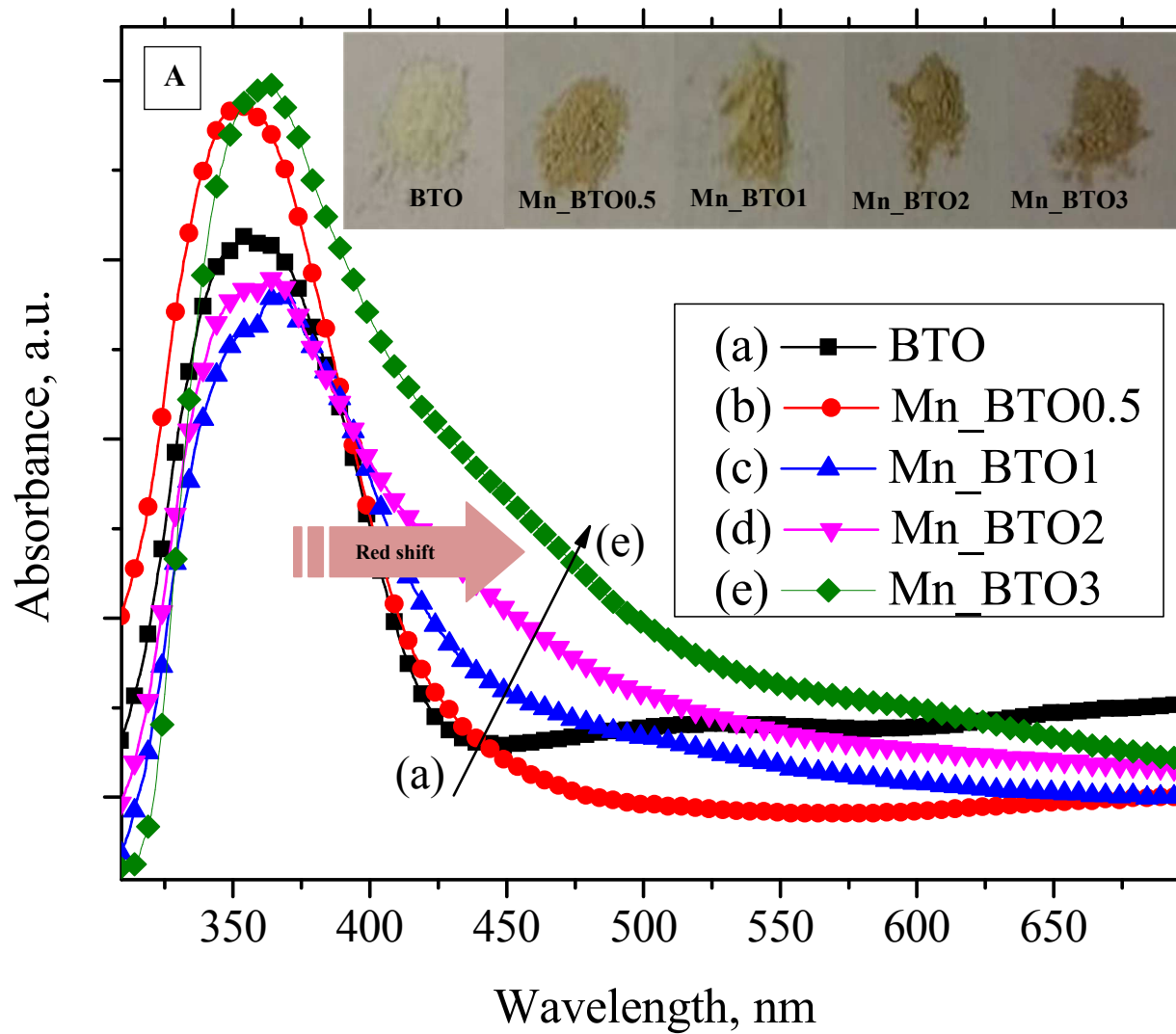


Fig. 3 (A) The TEM image of a cluster of Mn_BTO1 and a magnified image of one of the particles, indicating a size of 25 ± 5 nm. **(B)** The HRTEM image of the Mn_BTO1 particle indicating the crystalline nature of the material. The inset of **(B)** shows the high resolution fast Fourier transformation (FFT) analysis of the Mn_BTO1.



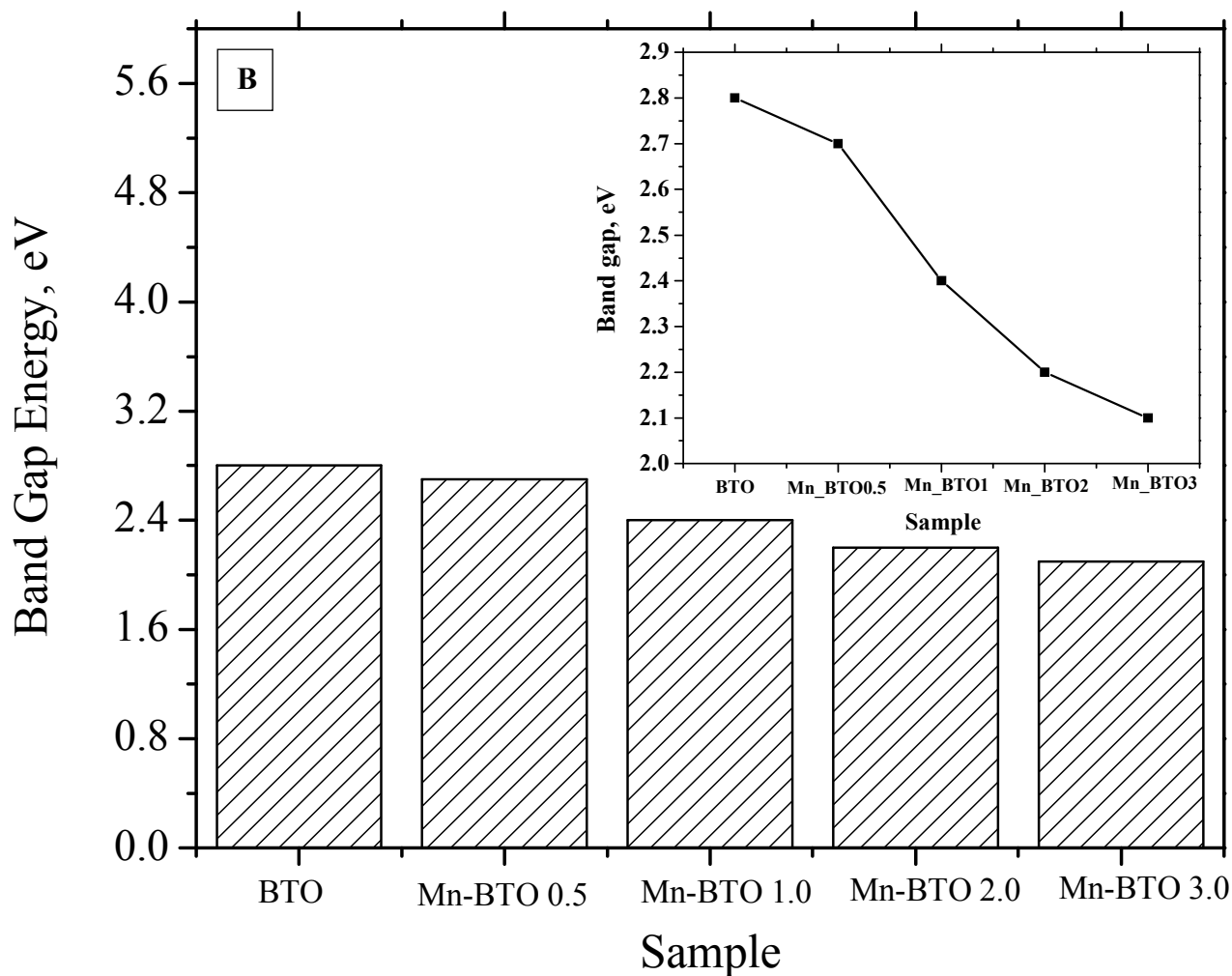


Fig. 4 (A) The UV-Visible spectra of (a) BTO and Mn_BTO catalysts indicating a gradual red shift in the absorbance onset with various Mn content of (b) 0.5 wt%, (c) 1 wt% (d) 2 wt%, and (e) 3 wt%. The inset of the figure shows a collage of photographs of BTO with varying Mn content indicating gradual darkening consistent with the absorbance spectra **(B)** The Bandgap variation of BTO and Mn_BTO as a function of manganese concentration (Inset: Linear reduction of band gap with the increase in manganese concentration)

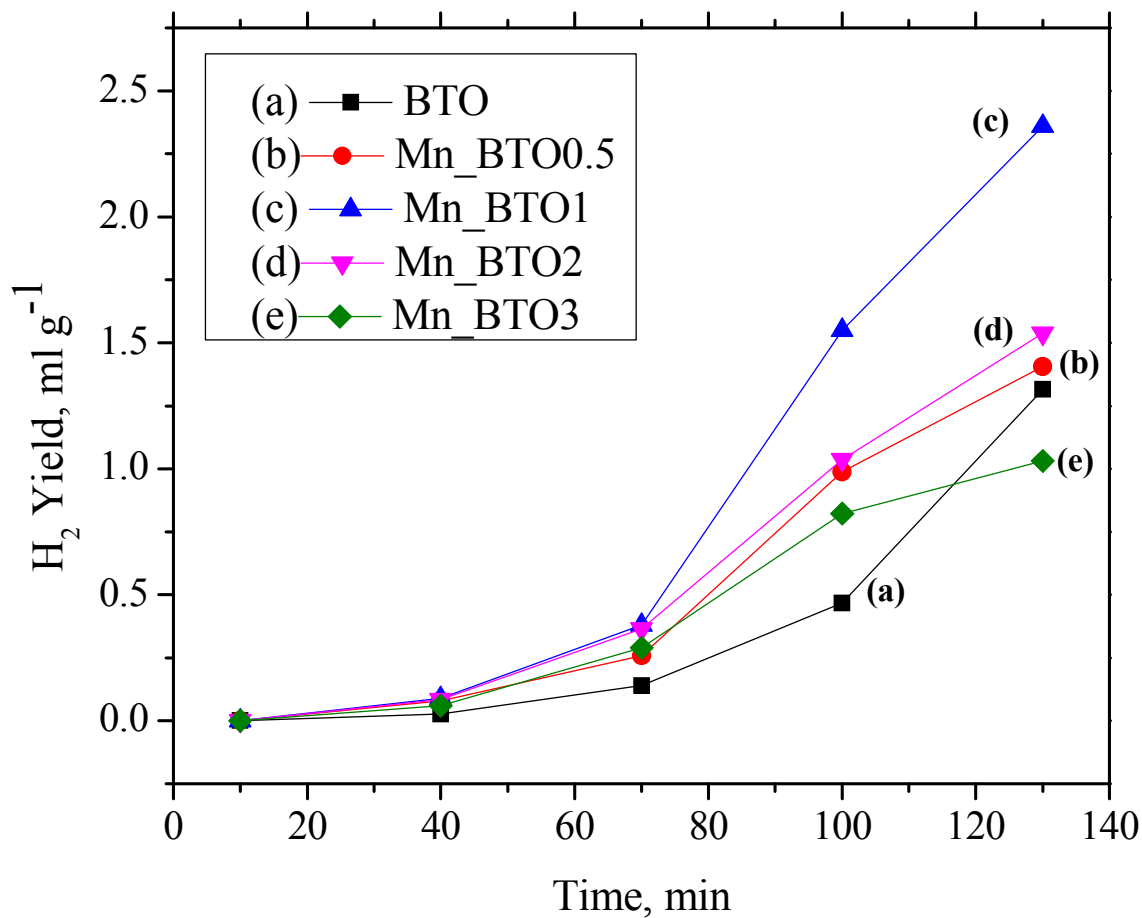


Fig. 5 The time resolved hydrogen yield obtained using (a) BTO and Mn-BTO with varying Mn content of (b) 0.5 wt%, (c) 1 wt%, (d) 2 wt%, and (e) 3 wt%. The experiment was carried out in a water-methanol mixture of 250/50 (V/V) and using a UV-visible light source in a slurry reactor.

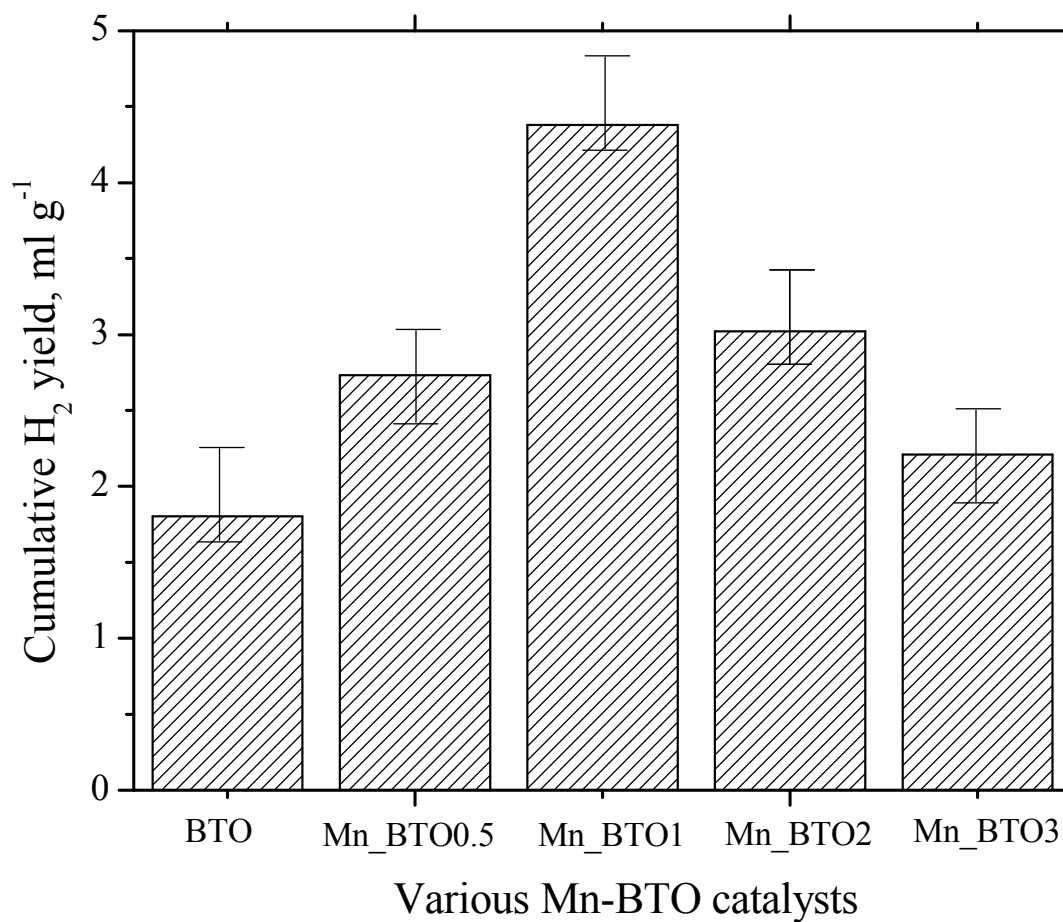


Fig 6. The cumulative hydrogen yield obtained using the BTO and Mn_BTO with varying Mn content over a 2 hour duration. The hydrogen was generated from a water-methanol mixture of 250:50 in a slurry reactor. The illumination was performed using a UV-visible light source.

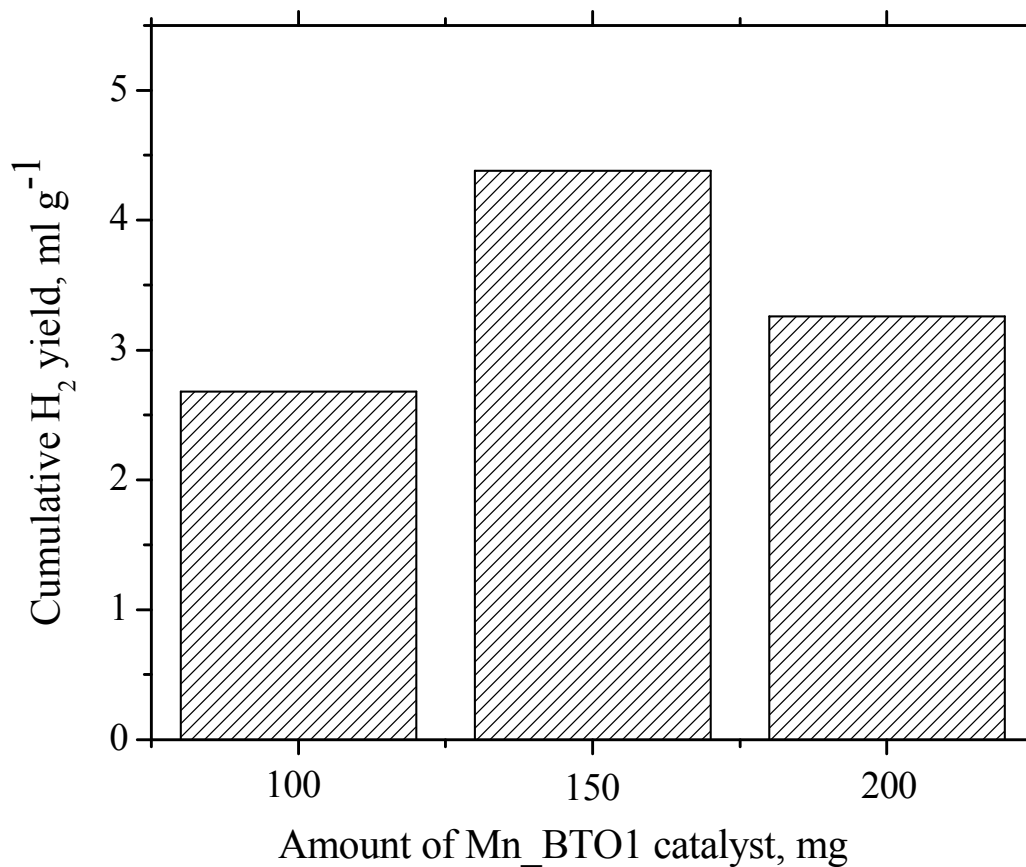


Fig. 7 The effect of the catalyst loading was examined with 1 wt% Mn (Mn_BTO1) in the presence of a water: methanol mixture of 250/50 (V/V) in the slurry reactor. The cumulative yield at the end of 2.16 h is shown.

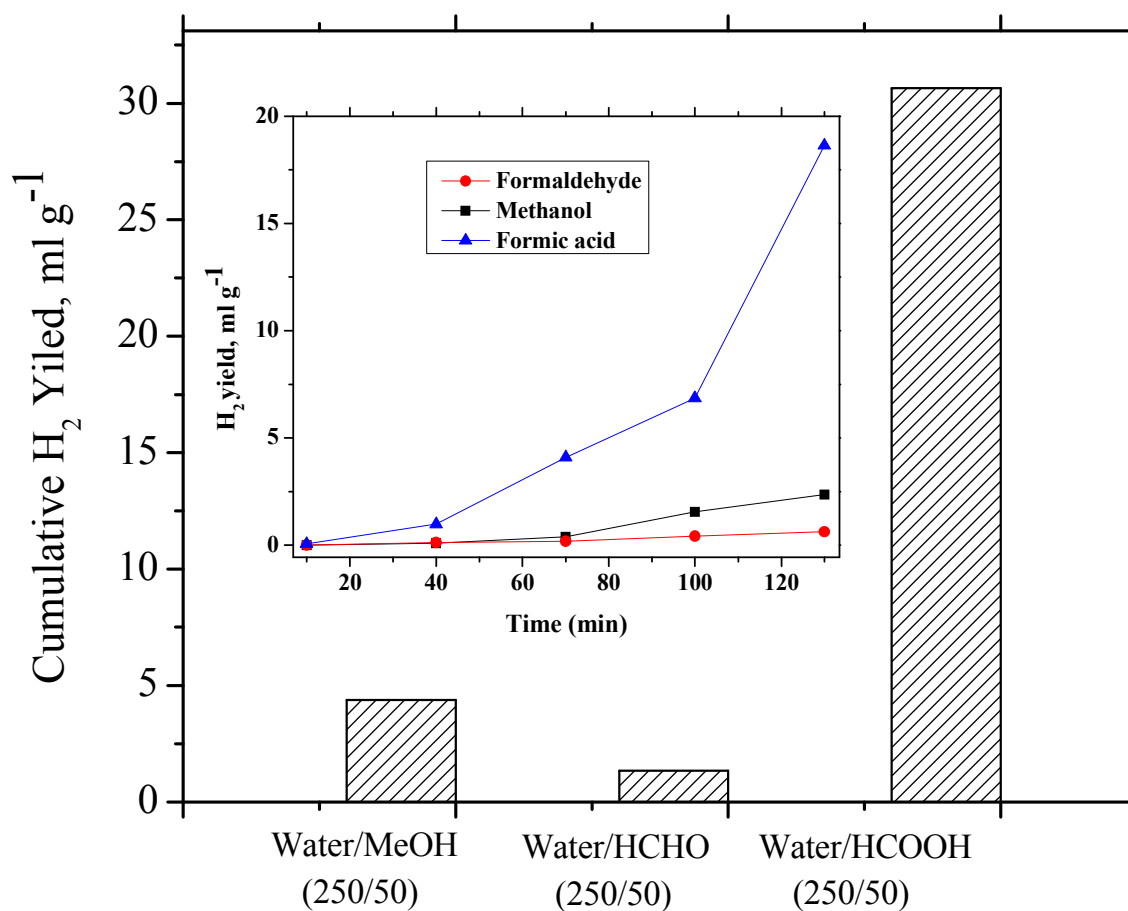


Fig. 8 Cumulative hydrogen yield with various wastes as additive using Mn_BTO1 catalyst. (Inset: Time resolved hydrogen yield)

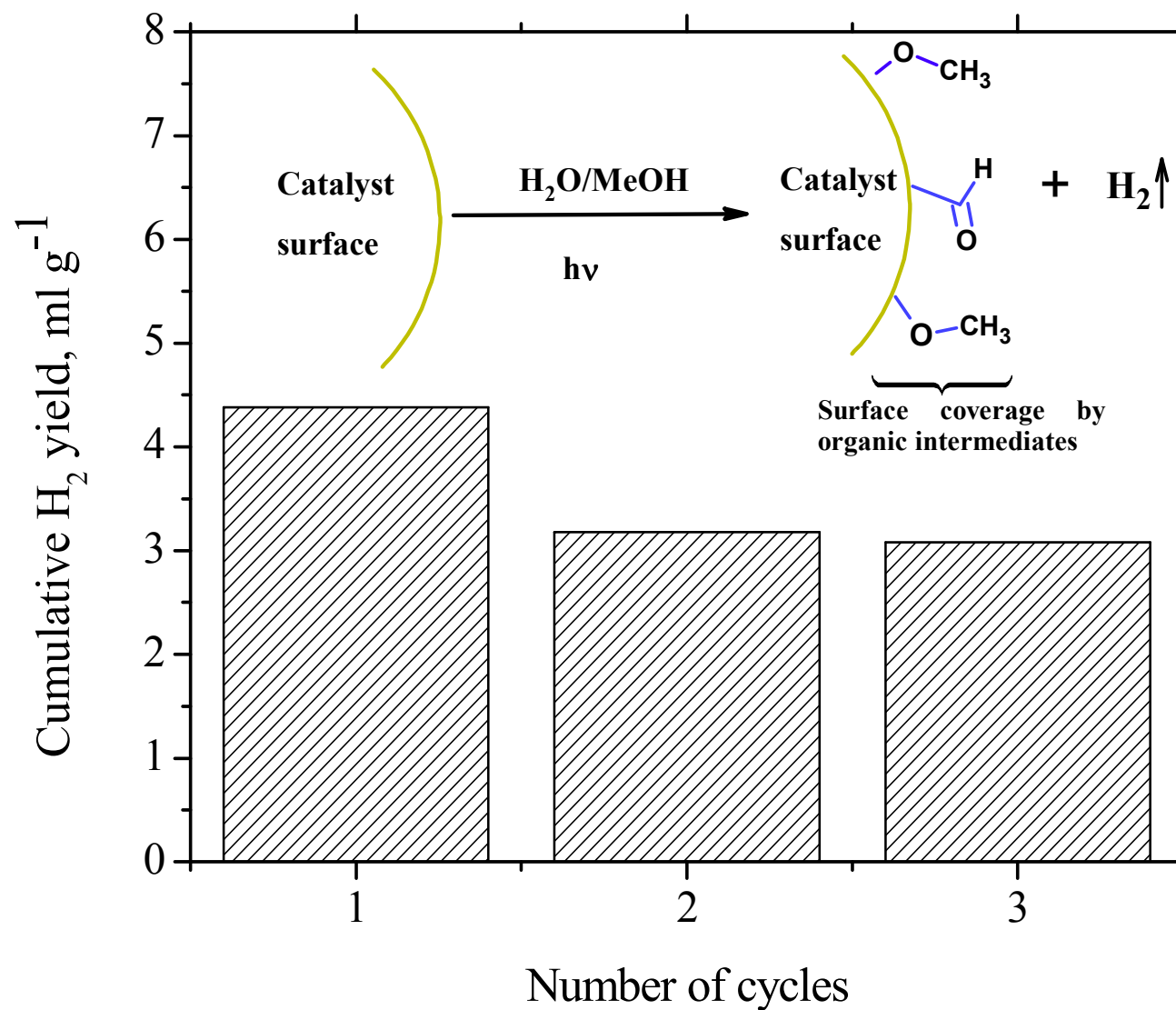
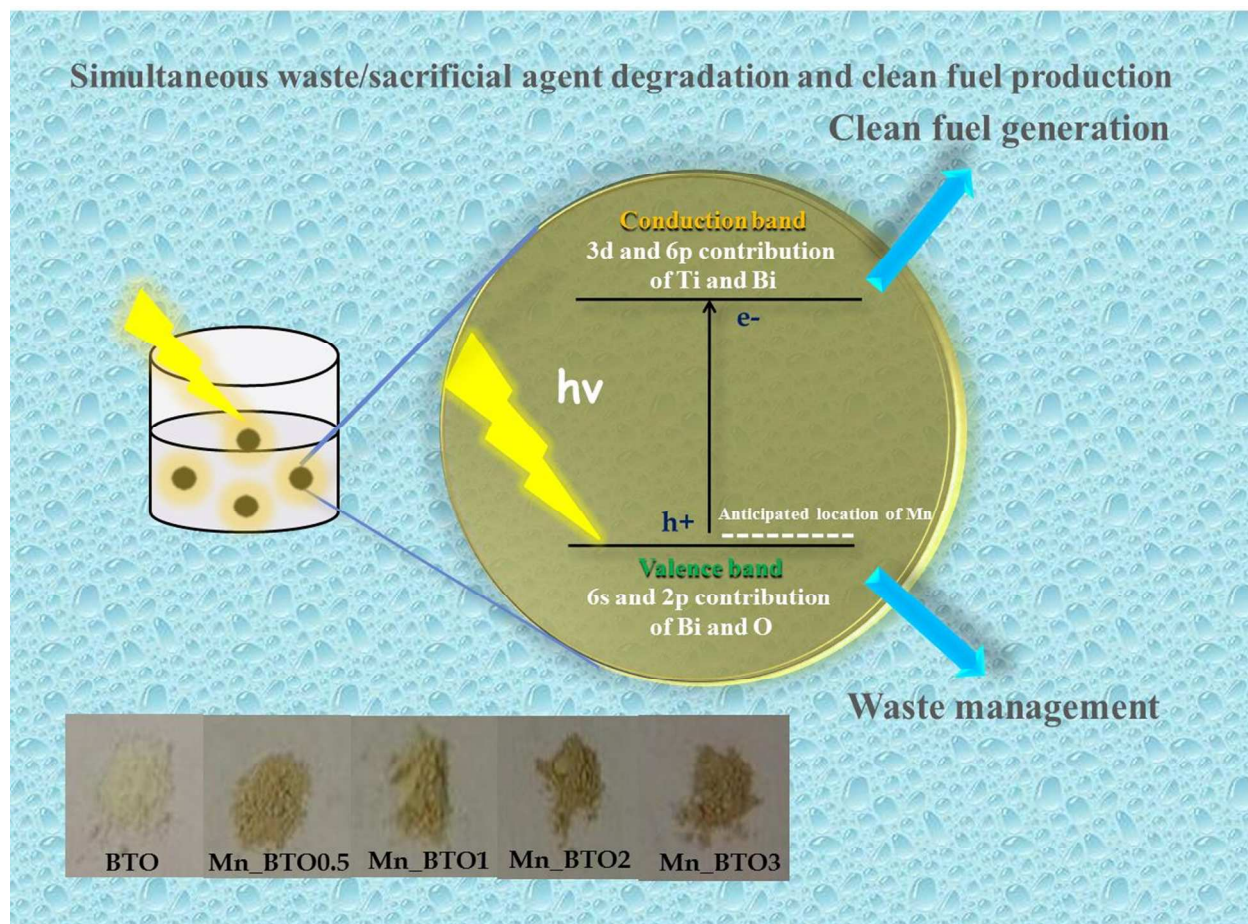


Fig. 9 The studies on the reusability of the catalyst Mn_BTO1. (Inset: Showing reason for the decrease in the catalyst surface activity after one run)



Graphical Abstract The applicability of pyrochlore bismuth titanate as a photocatalyst amenable to additional element inclusion resulting in a bandgap engineered composite oxide nanostructure (BECON) offers significant potential to multifunctional photo-driven applications.